Rag GTPases Suppress Renal Cystic Disease by Inhibiting TFEB Independently of mTORC1

Short title: Rag GTPases are Suppressors of Renal Cystogenesis

Authors

Flaviane de Fatima Silva[1], Alexander R. Boucher Jr.[1], Huawei Li[1,†], Qingbo Chen[1,†], Maria Gaughan[1], Ekaterina D. Korobkina[1], Marie Sophie Isidor[1,‡], Abigail O. Smith[1,§], Kuang Shen[1], Derek B. Allison[2], Pamela V. Tran[3], Gregory J. Pazour[1], David A. Guertin[1*]

Affiliations

[1] Program in Molecular Medicine, University of Massachusetts Chan Medical School, Worcester, MA, 01605.
[2] Department of Pathology & Laboratory Medicine, University of Kentucky, Lexington, KY, 40536.
[3] Department of Cell Biology and Physiology, The Jared Grantham Kidney Institute, University of Kansas Medical Center, Kansas City, KS, 66160.
[‡] Novo Nordisk Foundation Center for Basic Metabolic Research, University of Copenhagen, Copenhagen, Denmark.
[§] Boston Combined Residency Program in Pediatrics, Boston Children's Hospital, Boston Medical Center, Boston, MA, 02115.

[†] These authors contributed equally.

Corresponding author:
David A. Guertin, PhD
Professor, Program in Molecular Medicine, UMass Chan Medical School
366 Plantation St, N4-1099
Worcester, MA 01605
Phone: +1 (508) 856-8064
E-mail: david.guertin@umassmed.edu

Abstract

Aberrant mTORC1 activation in renal tubular epithelial cells (rTECs) is implicated as a critical driver of renal cystic diseases (RCDs), including autosomal dominant polycystic kidney disease (ADPKD) and tuberous sclerosis (TSC), yet its precise role remains unclear. Rag GTPases recruit mTORC1 to lysosomes, its intracellular activation site. Unexpectedly, we found that deleting *RagA/B* in rTECs, despite inhibiting mTORC1, triggers renal cystogenesis and kidney failure. We identify TFEB as the key driver of cystogenesis downstream of *RagA/B* loss and show that Rag GTPases, rather than mTORC1, are the primary suppressors of TFEB *in vivo*. We further highlight increased nuclear TFEB as a shared feature of several RCD models, whereas differences in mTORC1 activity may explain variable mTORC1 inhibitor efficacy. Finally, we provide evidence that nuclear TFEB, rather than mTORC1 activation, is a more consistent biomarker of cyst-lining epithelial cells in ADPKD. Overall, these findings challenge the prevailing view that mTORC1 hyperactivation is required for renal cystogenesis, which has important translational implications.

Keywords: Rag GTPase, mTORC1, TFEB, renal cystogenesis, ADPKD, TSC, UCP1

Teaser

A serendipitous finding uncovers the Rag GTPases as strong suppressors of renal cystogenesis with important disease implications.

Introduction

Aberrant activation of mechanistic target of rapamycin complex 1 (mTORC1) has long been considered the key driver of renal cystic diseases (RCD), including autosomal dominant polycystic kidney disease (ADPKD) and tuberous sclerosis complex (TSC)-associated renal disease [1]. However, the precise mechanisms by which mTORC1 signaling drives cystogenesis remain poorly defined. Nevertheless, the mTORC1 inhibitor rapamycin and its analogs are under investigation as potential therapies for RCDs, including ADPKD. Yet, despite promising results in preclinical ADPKD models, human trials have shown minimal benefit for reasons that remain unclear [2], suggesting critical gaps in the understanding of mTORC1-driven renal cystogenesis.

mTORC1 is a master regulator of cell growth and metabolism that becomes dysregulated in many human conditions, including cancer, diabetes, and aging-related pathologies. mTORC1 promotes cell growth by stimulating anabolic pathways, such as protein, lipid, and nucleic acid biosynthesis through its canonical substrates, S6K and 4E-BP1 [3]. mTORC1 also facilitates growth by suppressing catabolic pathways like autophagy by directly phosphorylating and inhibiting the ULK1 complex [4], and by directly phosphorylating and inhibiting Transcription Factor EB (TFEB), a transcriptional activator of autophagy, lysosomal biogenesis, and metabolic genes [5]. The activation of mTORC1 occurs at lysosomes in response to both nutrients and growth factors.

Mechanistically, nutrients such as amino acids stimulate mTORC1 recruitment to the lysosome via the Rag GTPase, a heterodimer composed of RagA or RagB and RagC or RagD, that is anchored to the lysosomal surface by Ragulator [6]. At the lysosome, mTORC1 is catalytically activated by Rheb, another lysosomal GTPase that is inhibited by the TSC complex and stimulated by growth factors [7]. Thus, the Rag-Regulator complex is considered the central organizer of mTORC1 activation, ensuring that mTORC1 is only activated when both sufficient nutrients and growth factors are present [8].

In this study, we describe an unexpected mouse model of renal cystic disease caused by the deletion of *RagA* and *RagB* in renal tubular epithelial cells (rTECs). This finding was surprising because *RagA/B* loss inhibits Rag GTPase-dependent mTORC1 activation, which is expected to suppress, rather than promote, cystogenesis. We provide evidence that TFEB activation downstream of *RagA/B* loss is sufficient to drive cystogenesis despite simultaneously inhibiting mTORC1. Our findings further reveal that Rag GTPases, rather than mTORC1 itself, serve as the primary negative regulators of TFEB in rTECs. We also find that aberrant TFEB nuclear localization—rather than aberrant mTORC1 activity—is a more consistent biomarker of the cyst-lining epithelial cells in human ADPKD samples. These results advance a new mechanistic understanding of the Rag-GTPase-mTORC1-TFEB signaling axis *in vivo* and highlight TFEB and its upstream regulatory pathways as potential therapeutic targets for renal cystic diseases, including ADPKD [9].

Results

RagA/B deletion in rTECs causes polycystic kidney disease

While investigating Rag GTPase function in UCP1-positive brown adipocytes, we unexpectedly discovered that *Ucp1*-Cre;*RagA/B* male mice develop kidney cysts by 4 weeks of age, which progresses to severe polycystic kidney disease by 12 weeks [Fig. S1A-C], indicated by H&E staining [Fig. S1B] and increased kidney to body weight ratio [Fig. S1C]. Cystogenesis occurred in the kidney cortex and medulla [Fig. S1D] and was associated with fibrosis [Fig. S1E], inflammation [Fig. S1F], and elevated blood urea nitrogen (BUN) levels [Fig. S1G]. A comparative analysis of 8-week-old female *Ucp1*-Cre;*RagA/B* mice also showed cyst formation with slightly less severity [Fig. S1H-K]. This was unexpected: First, because UCP1 expression is widely considered specific to brown/beige adipocytes; second, because mTORC1 activation is considered necessary for renal cystogenesis, and deleting *RagA/B* inhibits mTORC1.

To explain why *Ucp1*-Cre*;RagA/B* mice develop polycystic kidneys, we did PCR genotyping, which showed Cre-mediated recombination of the *RagA* and *RagB* floxed alleles in whole kidney samples [Fig. S2A]. Cell labeling with *Ucp1*-Cre*;mTmG* reporter mice, in which Cre induces indelible mGFP expression, pinpointed Ucp1-Cre recombination to rTECs in the medulla and some in the cortex [Fig. S2B]. Labeling with

124 *Ucp1*-Cre*;mTmG*;*RagA/B* mice additionally localized Cre-mediated mGFP expression to
125 epithelial cells lining the cysts [Fig. S2C]. Whole tissue Western blots from wild type and
126 *Ucp1*$^{-/-}$ mice confirmed UCP1 protein expression in the kidney of 1-week-old mice [Fig.
127 S2D], and UCP1 co-immunofluorescence with aquaporin 2 (AQP2) localized its
128 expression to the collecting duct in 1-week-old mice [Fig. S2E]. These data suggested that
129 *Ucp1*-Cre-mediated deletion of *RagA/B* in kidney TECs was the cause of polycystic
130 kidney formation.
131
132 To confirm that Rag GTPase inhibition specifically in rTECs drives cystogenesis,
133 we generated *Cadherin 16/Ksp*-Cre*;RagA/B* mice (hereafter *Ksp*-Cre*;RagA/B*), which
134 conditionally delete *RagA/B* in distal tubular epithelial cells and collecting duct cells [10].
135 Strikingly, all *Ksp*-Cre*;RagA/B* male and female mice developed renal cysts with similar
136 trajectories [Fig. 1A-C, Fig. S3A-C]. Kidneys were visibly larger at 6 weeks in the *Ksp-*
137 *Cre;RagA/B* mutants [Fig. 1A, Fig. S3A] and cyst formation was detectable by 4 weeks
138 [Fig. 1B, Fig. S3B]. Kidney to body weight ratio substantially increased from 4 through
139 12 weeks in the *Ksp*-Cre*;RagA/B* mice [Fig. 1C, Fig. S1C] with cyst formation equally
140 distributed throughout the cortex and medulla [Fig. 1D, Fig. S3D]. In males, fibrosis is
141 detectable by 8 weeks [Fig. 1E], correlating with a robust immune response [Fig. 1F], and
142 blood urea nitrogen (BUN) levels that are 2.9-fold higher than controls by 12 weeks [Fig.
143 1G] indicating kidney failure. All *Ksp*-Cre*;RagA/B* male mice have a shortened lifespan,
144 succumbing to renal failure between 4-6 months of age [Fig. 1H]. No renal cysts or kidney
145 failure were detected in *Ksp*-Cre*;RagA* or *Ksp*-Cre*;RagB* single knockout mice through 24
146 weeks, indicating compensation in suppressing renal cystogenesis [Fig. S4A-H].
147 Collectively, these data uncover RagA/B as potent suppressors of kidney cystogenesis.
148
149 ***RagA/B* loss causes cystogenesis despite inhibiting mTORC1**
150
151 Aberrant mTORC1 activation is a hallmark of polycystic kidney diseases [1]; thus,
152 it was unexpected that deleting *RagA* and *RagB*—essential components of the Rag
153 GTPase complex that activate mTORC1—induces cystogenesis. We confirmed decreased
154 *RagA* and *RagB* mRNA and protein expression in kidneys from *Ksp*-Cre*;RagA/B* mice
155 [Fig. 2A, 2B]. The residual expression likely reflects non-targeted cell populations present
156 in whole kidney samples, which presents an obstacle for determining the effects of
157 *RagA/B*-deletion on mTORC1 activity specifically in the rTECs. For example, Westerns
158 using whole kidney tissue lysates show total protein upregulation of the mTORC1
159 substrates S6K and 4E-BP1, as well as AKT in the mutant kidneys [Fig. 2B], hinting at
160 broader tissue-wide effects beyond the rTEC subpopulation.
161
162 To circumvent this caveat and examine mTORC1 activity specifically in the rTECs
163 that are targeted by Ksp-Cre, we performed immunohistochemistry (IHC).
164 Phosphorylated-S6 (p-S6), a target of S6K and a robust *in vivo* mTORC1 reporter, was
165 absent in most of the cyst lining TECs in the medulla and cortex of *Ksp*-Cre*;RagA/B* mice
166 at 2, 4, and 8 weeks [Fig. 2C], consistent with mTORC1 inactivation. We also detected
167 mildly elevated p-AKT in *Ksp*-Cre*;RagA/B* rTECs at 4 and 8 weeks [Fig. S5A], which is

another indicator of decreased mTORC1 signaling caused by loss of feedback inhibition of the PI3K/AKT pathway [11-13]. Additionally, we noted a significant increase in p-S6 in the non-targeted interstitial cells, uncovering a secondary response triggered by an unknown mediator of cell crosstalk [Fig. S5B]. Nevertheless, these data indicate that renal cysts form in *Ksp*-Cre*;RagA/B* mice despite mTORC1 inhibition in rTECs.

RagA/B suppresses TFEB activation in rTECs

Next, we investigated the effects of *RagA/B* loss on TFEB [14-16]. Inhibition of TFEB by direct mTORC1 phosphorylation at the lysosome is considered the main mechanism of preventing TFEB nuclear localization and gene activation [17]. It was also recently shown that TFEB is recruited to mTORC1 via a direct interaction with Rag-GTPase [18], which is different from how canonical mTORC1 substrates like S6K and 4E-BP1, which contain a TOR-signaling (TOS) motif, are recruited to mTORC1 [19-21]. In normal rTECs, TFEB is primarily cytosolic or distributed between cellular compartments [Fig. 3A]. Strikingly, in the *Ksp*-Cre*;RagA/B* mice, TFEB is concentrated in the nucleus of nearly all cyst-lining TECs during early cyst formation (2 weeks), and it becomes more prominent in the nucleus as the disease progresses (4 and 8 weeks) [Fig. 3A], which correlates with an increase in total TFEB protein levels in whole kidney lysates [Fig. 2B].

Consistent with TFEB activation in *Ksp*-Cre*;RagA/B* mutant kidneys, bulk RNA-sequencing shows upregulation of direct TFEB target genes, called Coordinated Lysosomal Expression and Regulation (CLEAR) genes, in the cystic kidneys [22] [Fig. 3B], noting that a subset of CLEAR genes also decreases [Fig. 3B], indicated by group I and II genes, respectively. Analysis of the broader TFEB target gene network (also called the CLEAR network) showed a similar pattern [Fig. S6A]. We also observe increased WNT/β-catenin signaling, which has been associated with increased TFEB activation [23], indicated by an increase in WNT target gene expression in cystic kidneys [Fig. 3C], increased β-catenin expression in whole tissue lysates [Fig. 3D], and β-catenin localization to adherens junctions in the mutant rTECs [Fig. 3E]. These data suggest that RagA/B is a key suppressor of TFEB and WNT activation *in vivo*.

Reduced efficacy of rapamycin in *Ksp*-Cre;*RagA/B* mice compared to *Ksp*-Cre;*Tsc2* mice

Several preclinical studies show that rapamycin reduces cyst formation across multiple models of RCD [24]. Rapamycin is particularly effective at reducing cystic burden in *Ksp*-Cre*;Tsc2* kidneys, a model of renal cystogenesis in tuberous sclerosis associated with aberrant activation of both mTORC1 and TFEB [24]. In this model, rapamycin completely relieved cystic burden and corrected both aberrant mTORC1 activation and TFEB nuclear localization, leading to a model in which high mTORC1 activity promotes TFEB nuclear localization by an unknown mechanism to drive cystogenesis [24]. We compared our whole kidney bulk RNA-seq data from the *Ksp*-Cre*;RagA/B* mice to published bulk RNA-seq data from the kidneys of age-matched *Ksp*-

212 Cre*;Tsc2* mice [24], which showed remarkable similarity [Fig. 4A]. The similarity in gene
213 signatures was surprising given that mTORC1 is inhibited by RagA/B loss while
214 mTORC1 is activated by TSC2 loss; nevertheless, the similarity suggests at least partial
215 overlapping molecular pathology.
216
217 This raised the question of whether rapamycin might be effective at reducing
218 cystic burden in the *Ksp*-Cre*;RagA/B* mice. We hypothesized that rapamycin would be
219 less effective in the *Ksp*-Cre*;RagA/B* model because mTORC1 is already inhibited by
220 RagA/B loss. To test this, we treated *Ksp*-Cre*;RagA/B* and littermates floxed controls with
221 Rapamycin (1.0 mg/Kg) from P25 to P50 [Fig. 4B] following the exact protocol
222 previously shown to be effective at reverting kidney cysts in *Ksp*-Cre*;Tsc2* mice [24].
223 Consistent with our hypothesis, rapamycin offered no benefit in reducing kidney size or
224 cystogenesis in the *Ksp*-Cre*;RagA/B* mice when delivered using the same dose and
225 treatment regimen that was highly effective at reducing cystic burden in *Ksp*-Cre*;Tsc2*
226 mice [Fig. 4C, 4D]. By IHC, we observed that this rapamycin treatment regimen reduced
227 the pS6 signal detected in the interstitial cells of *Ksp*-Cre*;Tsc2* mice [Fig. 4D], but did not
228 affect TFEB nuclear localization, which remained nuclear [Fig. 4D]. This is consistent
229 with cystogenesis in both *Ksp*-Cre;*RagA/B* and *Ksp*-Cre;*Tsc2* mice being driven by
230 distinct mechanisms that converge on TFEB activation, and it reveals that not all
231 preclinical models of RCD are necessarily driven by aberrant mTORC1 activation and
232 thus may not respond equally to rapamycin treatment.
233
234 **_Tfeb_ is required for cyst formation downstream of _RagA/B_ loss**
235
236 In other models of renal cystogenesis, aberrant TFEB/TFE3 is thought to promote
237 cystogenesis by activating mTORC1 in a feedback activation loop [23-25]. Therefore, we
238 next asked whether TFEB was required for cystogenesis downstream of *RagA/B* loss, in
239 which mTORC1 is inhibited. For this, we generated *Ksp*-Cre*;RagA/B;Tfeb* triple knockout
240 (TKO) mice. Strikingly, at 6 weeks of age, there was no difference in kidney size between
241 control and TKO mice [Fig. 5A, 5B], no cysts were detected throughout the TKO kidneys
242 [Fig. 5C], and there were no signs of kidney dysfunction based on BUN levels, which
243 were similar to *wild-type* control [Fig. 5D]. IHC confirmed TFEB loss in rTECs,
244 especially in the medulla where collecting ducts and loop of Henle are located [Fig. 5E].
245 Using the TFEB target genes *Atg9b* and *Ctsd* as TFEB activity markers, we confirmed that
246 *Tfeb* deletion normalizes TFEB target gene expression [Fig. 5F]. *Tfeb* deletion also
247 normalized total S6K, 4E-BP1, and AKT protein levels in whole kidney lysates [Fig. 5G].
248 We noted that pAKT remained modestly elevated in mutant whole kidney lysates, which
249 is consistent with mTORC1 inhibition [Fig. 5G], which we confirmed by IHC for pS6 and
250 pAKT, respectively [Fig. 5H, 5I]. Thus, TFEB is required for cyst formation caused by
251 *RagA/*B loss.

Rag GTPase, not mTORC1, is the main TFEB suppressor *in vivo*

mTORC1 is widely considered the major negative regulator of TFEB activity [17]. However, *Ksp*-Cre*;Raptor* mice, which are predicted to both inhibit mTORC1 and trigger nuclear TFEB, just like the *Ksp*-Cre*;RagA/*B mice, have visibly smaller kidneys with no cysts and normal BUN levels [Fig. 6A-D] [26]. As expected, deleting *Raptor* both decreased pS6 and increased pAKT in rTECs, respectively [Fig. 6E, 6F]. However, TFEB did not accumulate in the nucleus of *Raptor* mutant rTECs [Fig. 6G], and the mRNA *Atg9b* and *Ctsd* were not elevated by *Raptor* loss [Fig. 5F]. Notably, the total protein levels of S6K and 4E-BP1 were elevated in *Ksp*-Cre*;Raptor* mutant whole kidneys [Fig. 6H], like in the *Ksp*-Cre*;RagA/*B mice [Fig. 2B], suggesting this phenomenon is more linked to impaired Rag-GTPase and/or mTORC1 activity but not TFEB activation. Overall, the observation that both *Ksp*-Cre*;RagA/B* and *Ksp*-Cre*;Raptor* models reduce mTORC1 signaling, but only *RagA/B* deletion activates TFEB, underscores TFEB activation as the critical driver of cystogenesis and reveals that, *in vivo*, Rag GTPases—not mTORC1—serve as the primary negative regulators of TFEB.

Nuclear TFEB is more consistent than pS6 as a biomarker in ADPKD

We also compared bulk RNA-seq data from *Ksp*-Cre;*RagA/B* cystic kidneys to previously published RNA-seq data from kidneys of postnatal day 7 (*P7*) *HoxB7*-Cre;*Pkd1* and *HoxB7*-Cre;*Pkd2* mice [27], established ADPKD models with reasonably well-matched bulk RNA-seq data. This analysis also revealed remarkable similarity in gene signatures between the *RagA/B* mutant kidneys and both the *Pkd1* and *Pkd2* mutant gene signatures [Fig. 7A]. Epithelial-mesenchymal transition (EMT), E2F targets, IL6/JACK-STAT signaling, TGFβ signaling, and WNT/β-catenin signaling were among the commonly upregulated pathways with established links to ADPKD [28]. We also generated a PKD-hallmark gene set based on published genes associated with ADPKD models [Fig. 7B]. Most of the genes we identified showed directional changes in the *RagA/B* mutant kidneys that are consistent with ADPKD, including increases in *Tacstd2* and *Gprc5a* expression [29]. This overlap between *Ksp*-Cre*;RagA/B* kidneys and models of ADPKD, in addition to TSC, implicate deregulation of TFEB as a shared feature of different renal cystic diseases, as suggested recently [30]. A recent single-cell RNA-sequencing study using human ADPKD samples also identified TFEB target genes as being significantly upregulated [31].

To investigate this further in ADPKD, we compared TFEB nuclear localization to pS6 as biomarkers of renal cystic cells in the *Pax8-rtTA;Tet-O-7*-Cre*;Pkd1* model, a widely accepted preclinical mouse model of ADPKD [31, 32]. This revealed a heterogeneous labeling pattern; for example, some cystic cells showed strong nuclear TFEB signal but little to no pS6 [Fig. 7C]—a pattern consistent with the *Ksp*-Cre*;RagA/B* model. Other cyst-lining cells showed elevated total TFEB protein that was distributed between both the nucleus and cytosol, which also had elevated pS6 [Fig. 7C]. These data hint at temporal and/or spatial differences in how mouse rTECs may reprogram mTORC1

296 and TFEB activity in response to *Pkd1* loss. Nevertheless, it confirms aberrant TFEB
297 expression as a prominent biomarker in a pre-clinical model of ADPKD.
298
299 Finally, we examined three human ADPKD kidney sections from two patients with
300 PKD1 mutations and a third patient with a family history of *PKD1* mutations. In all three
301 cases, aberrant TFEB nuclear localization was consistently present in the cyst-lining
302 epithelial cells [Fig. 7D]. However, the pS6 signal was inconsistent. For example, in the
303 patient 1 samples, we observed high nuclear TFEB that overlapped with high pS6; but in
304 patient 2 and 3 samples, we observed nuclear TFEB but no pS6, which resembles the
305 pattern we observed in *Ksp*-Cre*;RagA/B* model. Thus, aberrant TFEB activation may be a
306 more consistent biomarker of late-stage ADPKD than aberrant mTORC1 activation,
307 warranting a deeper investigation into the function of the Rag-GTPase/TFEB pathway in
308 ADPKD.
309
310 **Discussion**
311
312 Aberrant mTORC1 activation is widely considered a hallmark driver of renal
313 cystic diseases (RCDs), including ADPKD and TSC. However, its precise molecular role
314 in cyst formation and whether it functions similarly across different types of RCDs has
315 remained unclear. In this study, we discovered that RagA and RagB, which are required
316 for RagC and RagD activity and mediate mTORC1 activation at lysosomes [8], function
317 as redundant suppressors of renal cystogenesis. This demonstrates that the conventional
318 Rag GTPase-activated mTORC1 pathway is not essential for renal cystogenesis. Instead,
319 we show that TFEB drives cyst formation downstream of Rag GTPase loss, independent
320 of hyperactivation of the canonical Rag GTPase-mTORC1 pathway. These findings
321 highlight the broad relevance of TFEB—both functionally and as a biomarker—in RCDs
322 and underscore key gaps in understanding if and how to target the mTORC1 pathway
323 across different RCD subtypes.
324
325 Another key finding is that Rag GTPases, rather than mTORC1, serve as the
326 primary negative regulators of TFEB in rTECs *in vivo*. This was uncovered by showing
327 that Raptor loss, unlike RagA/B loss, results in minimal changes in TFEB localization *in*
328 *vivo*. This was surprising because the prevailing model, based largely on *in vitro* studies,
329 is that mTORC1-dependent phosphorylation of TFEB is the primary mechanism
330 restricting its nuclear localization and activity [17]. Recent structural data indicate that
331 RagA and RagC directly interact with TFEB, in addition to mTORC1, to facilitate their
332 interaction at lysosomes [33], which is different than how S6K and 4E-BP1 interact with
333 mTORC1 [34]. However, our genetic data suggest that direct interaction between Rag
334 GTPase and TFEB may be the dominant mechanism restraining TFEB nuclear localization
335 *in vivo*, with mTORC1-dependent phosphorylation being an auxiliary mechanism to fine-
336 tune TFEB activity. *In vitro*, siRNA knockdown of *Raptor* in human retinal pigment
337 epithelial cells induced TFEB nuclear localization [16], seemingly at odds with our *in vivo*
338 findings. However, that study also reported that *Raptor* knockdown caused a substantial
339 fraction of TFEB to redistribute to lysosomes. One possibility is that Raptor loss frees up

340 TFEB binding sites at lysosomes, and *in vivo*—within a physiologically relevant
341 context—this lysosomal sequestration may be sufficient to restrain pathological TFEB
342 activation, even when mTORC1-dependent TFEB phosphorylation is inhibited. Another
343 possibility is that a compensatory kinase or other mechanism may substitute for mTORC1
344 in phosphorylating and inhibiting TFEB upon *Raptor* loss. Future biochemical and genetic
345 studies will be needed to test these hypotheses.
346
347 We also show that the cystic kidneys in *Ksp*-Cre*;RagA/B* mutants show
348 considerable molecular overlap with models of renal cystogenesis in TSC (*Tsc2* loss) and
349 ADPKD (both *Pkd1* and *Pkd2* loss), including aberrant TFEB activation [30, 35, 36],
350 suggesting TFEB activation is a common denominator across several RCDs, while
351 mTORC1's role may be more variable. Genetic studies in mice support a critical role for
352 TFEB in TSC [18, 35], and in Birt-Hogg-Dubé Syndrome, another rare genetic disorder
353 associated with increased risk of kidney cancer [25]. A functional role for TFEB in
354 ADPKD remains elusive. Nevertheless, these findings substantiate the potential value of
355 targeting TFEB or its downstream effectors in RCDs. It is interesting that a rapamycin
356 treatment regimen highly effective at reverting cysts in a *Ksp*-Cre*;Tsc2* model of renal
357 cystogenesis, also driven by TFEB activation, was ineffective in the *Ksp*-Cre*;RagA/B*
358 model. This aligns with our finding that TFEB, but not canonical mTORC1 signaling, is
359 essential for cystogenesis in *Ksp*-Cre*;RagA/B* mice and may hint at different pathological
360 mechanisms that converge upon TFEB activation.
361
362 A note on UCP1 in the kidney. The discovery that RagA/B suppresses renal
363 cystogenesis was serendipitous, arising from an unexpected phenotype following *Ucp1*-
364 Cre–mediated deletion of *RagA* and *RagB*. Although UCP1 is classically regarded as
365 specific to brown and beige adipocytes, multiple studies have hinted at its expression in
366 non-adipocyte cell types [37], including the kidney [37]. However, this has been debated
367 [38]. Here, using multiple protein-based assays and a *Ucp1* knockout control mouse, we
368 demonstrate UCP1 expression mainly in renal TECs of the collecting duct, explaining why
369 *Ucp1-Cre;RagA/B* developed renal cysts, and challenging the long-standing assumption
370 that UCP1 is restricted to adipose tissues. UCP1 expression in the kidney may have been
371 missed in other studies due to dynamic regulation, restricted expression to only a small
372 subset of cells, and/or to technical limitations of RNA sequencing, especially if its mRNA
373 expression is low. While a potential function for UCP1 in renal epithelial cells remains
374 unclear, it may relate to a role in mitigating mitochondrial stress [39]. Notably, human
375 UCP1 polymorphisms (e.g., 3826 A/G) have been linked to hypertension independent of
376 obesity [40, 41], raising the possibility of a previously overlooked role in kidney
377 physiology. Future studies are warranted to define whether UCP1 functions in this
378 context.
379
380 One limitation of our study is that it does not rule out the possibility of a non-
381 canonical Rag GTPase-independent mTORC1 pathway contributing to cyst formation in
382 *RagA/B*-deleted rTECs. Mounting evidence suggests that Rag GTPase–independent
383 mTORC1 signaling can occur, including *in vivo*; however, a consensus model and defined

functional role have yet to emerge [42-44]. Higher dosing of rapamycin and genetic ablation of Raptor in *Ksp*-Cre*;RagA/B* would help address this possibility. Overall, our findings that canonical mTORC1 signaling is not essential for renal cystogenesis underscore the critical need to further investigate the relative contributions of mTORC1, TFEB, and Rag GTPases across RCDs, including their temporal and spatial deregulation, to develop optimal treatments.

Materials and Methods

Animal studies

B6.Cg-Tg(Cdh16-cre)91Igr/J (strain #012237, hereafter named *Ksp-Cre*), C57BL/6J mice (stock #000664, hereafter named *wild type*), B6.129-Ucp1tm1Kz/J (Strain #:003124, hereafter named *Ucp1*$^{-/-}$), and *R26R-mTmG* (stock #007676) were purchased from The Jackson Laboratories. *Ucp1-Cre* mice (strain #024670) were provided by E. Rosen. *Tfeb*$^{fl/fl}$ mice were provided by E. Henske. *Ksp*-Cre*;RagA, Ksp*-Cre*;RagB*, *Ksp*-Cre*;RagA/B, Ksp*-Cre*;RagA/B;Tfeb, Ksp*-Cre*;Raptor, Ucp1*-Cre*;RagA/B, Ucp1*-Cre*;Raptor, Ucp1*-Cre*;mTmG*, and *Ucp1*-Cre*;RagA;RagB;mTmG* mice were generated by crossing in our facility. Mice were housed at 22 °C, in 50% ± 20% humidity, and a 12-h light–dark cycle, with free access to water and standard chow diet (Prolab Isopro RMH 3000). All experiments were approved by the UMass Chan Medical School IACUC (Protocol #202100035) and conducted with adherence to the National Institutes of Health Guide for the Care and Use of Laboratory Animals.

Treatment with rapamycin 1.0 mg/kg was performed as previously described [28], with 11 injections from P25 to P50. Paired control groups received vehicle (0.1% ethanol in sterile 0.9% NaCl). By the timepoints described (2 to 12 weeks old, or P50), the body weight was assessed, and euthanasia was performed by exsanguination (cardiac puncture under 2.0 % Isoflurane anesthesia) followed by cervical dislocation and kidney dissection. The euthanasia for all experiments was conducted at the same time of the day to minimize possible circadian variations, and all mice were in a fed state. The weight of the two kidneys was normalized and expressed as a percentage of body weight (Kidneys to body weight (%)). Blood samples were centrifuged for 10 minutes at 4 °C and 10.000 rpm, and the serum was aliquoted and kept at -80 °C until further analysis. Tissues were snap frozen using a liquid nitrogen-cooled Wollenburg clamp and transferred into 2-ml microcentrifuge tubes with a pre-cooled 5-mm metal bead. Tissues were homogenized using CryoMill (Retsch) at 25 Hz for 2 min. Tissue powder was weighed out into pre-cooled microcentrifuge tubes to be used in the analysis described below.

Tissue histology and Immunohistochemistry

Whole kidneys from all genotypes described were sectioned in the coronal plane and fixed in 10% formalin in PBS. Embedding, sectioning, and staining (H&E, Mason's Trichrome, and immunohistochemistry - IHC) were performed by the UMCMS Morphology Core facility. Paraffin-embedded kidney blocks from *Pkd1*$^{fl/fl}$ and *Pax8-rtTA;Tet-O-7*-Cre;*Pkd1*$^{fl/fl}$ mice were provided by the PKD Rodent Model Core of the Kansas PKD Research and Translational Core Center at KUMC (U54 DK126126) and the PKD Research Resource Consortium (PKD RRC). Kidney sections from ADPKD patients were provided by Derek B. Allison (University of Kentucky College of Medicine IRB # 79922; Table S1). For IHC, the sections were deparaffinized, rehydrated, submitted to antigen retrieval (10 mM Sodium Citrate buffer, pH 6.0), blocking of endogenous

434 peroxidase with 3% hydrogen peroxide solution, and then blocked with 5% goat serum.
435 The slides were incubated overnight (4 °C) with the primary antibodies p-S6-S240/244
436 (1:1000, 5364S, Cell Signaling), TFEB (1:100, 13372-1-AP, Proteintech), or p-Akt-S473
437 (1:200, 4058L, Cell Signaling). The sections were then washed and incubated with HRP-
438 conjugated Goat anti-Rabbit IgG secondary antibody (1:200, AS014, Abclonal),
439 developed with SignalStain® DAB Substrate (8059P, Cell Signaling), and mounted. Full
440 slide scans were taken at 20X using a Zeiss Axio-Scan.Z1. Zeiss Zen Blue 3.7 was used
441 for image acquisition and processing.
442
443 **Immunofluorescence**
444
445 Kidneys and BAT from *Ucp1*-Cre*;mTmG* and *Ucp1*-Cre*;RagA/B;mTmG* mice
446 were processed as previously described[45]. The slides containing frozen sections were
447 washed in PBS and mounted with Fluoromount-G with DAPI (00-4959-52, Invitrogen).
448 For UCP1 and Aquaporin 2 (AQP2) co-staining, the kidney sections were deparaffinized,
449 rehydrated, submitted to antigen retrieval with 10 mM Sodium Citrate buffer pH 6.0 at
450 120°C for 30 min, and blocked with 4% goat serum in 0.05% TBST with 0.1 % fish skin
451 gelatin and 0.1% Triton-X100. Primary antibodies UCP1 (1:500, ab10983, Abcam) and
452 aquaporin 2 – AQP2 (1:100, SAB5200110, Sigma), diluted in 0.05% TBST with 0.1%
453 fish skin gelatin were added overnight at 4 °C. The slides were incubated with the
454 secondary antibodies for 1 h at room temperature (Alexa Fluor 488 - A11008, 1:1000, and
455 Alexa Fluor 555- A-21428, 1:1000, Invitrogen). The slides were mounted with
456 Fluoromount-G with DAPI. All immunofluorescence images were taken at 10X or 20X
457 magnification using a Zeiss Confocal LSM 900+ Airyscan Microscope, and Zeiss Zen
458 Blue 3.7 was used for image processing.
459
460 **Blood Urea Nitrogen assessment**
461
462 The serum was diluted 1:1 with sterile 0.9% NaCl, and the urea was measured
463 following the urease method by a commercial kit (E-BC-K183-S, Elabscience). The assay
464 sensitivity is 0.114 mmol/L, inter-assay CV: 4.7%, and intra-assay CV: 4.6%. The Blood
465 urea nitrogen (BUN) final concentration was expressed as mmol/L.
466
467 **Gene expression analysis**
468
469 For qPCR, RNA was isolated from tissues using Qiazol (#79306, QIAGEN)-
470 chloroform and processed through RNeasy kit (#74106, QIAGEN). RNA (1.0 µg) was
471 reverse-transcribed to complementary DNA using a High-Capacity cDNA Reverse
472 Transcription kit (#4368813, Applied Biosystems). Quantitative PCR with reverse
473 transcription (qRT–PCR) was performed in 10-µl reactions using SYBR Green PCR
474 master mix (CW0955, CWBio). The reaction was performed using StepOnePlus (Applied
475 Biosystems), and melting curves were run on every plate for all genes to ensure efficiency
476 and specificity. TATA-box binding protein (*Tbp*), acidic ribosomal phosphoprotein P0

(*36b4*), and beta (β)-actin (*Actb*) gene expression geometric mean was used for normalization of each gene. The primer sequences used are listed in Table S2.

RNAseq

RNA-Seq analyses were performed on the ViaFoundry platform66 by Novogene. Briefly, sequence reads were processed with cutadapt (v4.4) to remove adapters and trim low-quality bases. Gene expression was quantified using salmon (v1.9.0) against the mouse genome assembly mm10 Gencode m25 basic gene annotation. Differential gene expression analyses were performed using DESeq2 (v1.40.2). Genes failing a minimum read count threshold (10 reads for each replicate in at least one condition) were removed before differential expression analysis. Gene set enrichment analysis was performed on preranked DESeq2-normalized RNA-seq data using GSEA Desktop v4.3.3 (build 16; Broad Institute, 4 Feb 2024) against the MSigDB Hallmark collection with 1,000 weighted gene-set permutations. All plots were generated using R packages ggplot2 (v.3.4.2), ggrepel (v0.9.3), and pheatmap (v1.0.12) or GraphPadPrism10.

Immunoblot analysis

Cryomilled samples from kidneys were lysed in RIPA buffer (150 mM NaCl, 50 mM HEPES at pH 7.4, 0.1% SDS, 1% Triton X-100, 1% glycerol, 2 mM EDTA, and 0.5% deoxycholate) containing protease and phosphatase inhibitor cocktail. Protein lysates were mixed with 5× SDS sample buffer, boiled at 95 °C, separated by SDS–PAGE, transferred to a polyvinylidene difluoride (PVDF) membrane, and subjected to immunoblot analysis. The primary and secondary antibodies and the respective dilutions used are listed in Table S3.

Statistical Analysis

Data were tested for distribution (Shapiro–Wilk test) and homogeneity of variances (F test). For comparisons between each genotype described and its respective floxed controls, unpaired Student t-test or Two-Way ANOVA, as indicated in the figure captions. In the t-test, when the F test was significant, the Welch correction was applied. The data are presented as mean ± standard error of mean (SEM), and the level of significance assumed was 5% ($p < 0.05$). All analyses were performed using GraphPad Prism 10.2.

513 **References**

514

515 1. Shillingford, J.M., et al., *The mTOR pathway is regulated by polycystin-1, and its*
516 *inhibition reverses renal cystogenesis in polycystic kidney disease.* Proc Natl Acad Sci U
517 S A, 2006. **103**(14): p. 5466-71.
518 2. Ravichandran, K., et al., *An mTOR kinase inhibitor slows disease progression in a rat*
519 *model of polycystic kidney disease.* Nephrol Dial Transplant, 2015. **30**(1): p. 45-53.
520 3. Saxton, R.A. and D.M. Sabatini, *mTOR Signaling in Growth, Metabolism, and Disease.*
521 Cell, 2017. **169**(2): p. 361-371.
522 4. Hosokawa, N., et al., *Nutrient-dependent mTORC1 association with the ULK1-Atg13-*
523 *FIP200 complex required for autophagy.* Mol Biol Cell, 2009. **20**(7): p. 1981-91.
524 5. Sardiello, M., et al., *A gene network regulating lysosomal biogenesis and function.*
525 Science, 2009. **325**(5939): p. 473-7.
526 6. Bar-Peled, L. and D.M. Sabatini, *Regulation of mTORC1 by amino acids.* Trends Cell
527 Biol, 2014. **24**(7): p. 400-6.
528 7. Menon, S., et al., *Spatial control of the TSC complex integrates insulin and nutrient*
529 *regulation of mTORC1 at the lysosome.* Cell, 2014. **156**(4): p. 771-85.
530 8. Valenstein, L.M., et al., *Rag–Ragulator is the central organizer of the physical*
531 *architecture of the mTORC1 nutrient-sensing pathway.* Proceedings of the National
532 Academy of Sciences, 2024. **121**(35).
533 9. Chebib, F.T. and V.E. Torres, *Autosomal Dominant Polycystic Kidney Disease: Core*
534 *Curriculum 2016.* Am J Kidney Dis, 2016. **67**(5): p. 792-810.
535 10. Thedieck, C., et al., *Expression of Ksp-cadherin during kidney development and in renal*
536 *cell carcinoma.* Br J Cancer, 2005. **92**(11): p. 2010-7.
537 11. O'Reilly, E.K., et al., *mTOR Inhibition Induces Upstream Receptor Tyrosine Kinase*
538 *Signaling and Activates Akt.* Cancer Research, 2006. **66**(3): p. 1500-1508.
539 12. Haar, V.E., et al., *Insulin signalling to mTOR mediated by the Akt/PKB substrate PRAS40.*
540 Nature Cell Biology, 2007. **9**(3): p. 316-323.
541 13. Sancak, Y., et al., *PRAS40 Is an Insulin-Regulated Inhibitor of the mTORC1 Protein*
542 *Kinase.* Molecular Cell, 2007. **25**(6): p. 903-915.
543 14. Malta, D.C. and A. Ballabio, *TFEB-mTORC1 feedback loop in metabolism and cancer.*
544 Cell Stress, 2017. **1**(1): p. 7-10.
545 15. Cui, Z., et al., *Structure of the lysosomal mTORC1–TFEB–Rag–Ragulator megacomplex.*
546 Nature, 2023. **614**(7948): p. 572-579.
547 16. Martina, A.J. and R. Puertollano, *Rag GTPases mediate amino acid–dependent*
548 *recruitment of TFEB and MITF to lysosomes.* Journal of Cell Biology, 2013. **200**(4): p.
549 475-491.
550 17. Martina, J.A., et al., *MTORC1 functions as a transcriptional regulator of autophagy by*
551 *preventing nuclear transport of TFEB.* Autophagy, 2012. **8**(6): p. 903-14.
552 18. Alesi, N., et al., *TSC2 regulates lysosome biogenesis via a non-canonical RAGC and*
553 *TFEB-dependent mechanism.* Nat Commun, 2021. **12**(1): p. 4245.
554 19. Schalm, S.S., et al., *TOS Motif-Mediated Raptor Binding Regulates 4E-BP1 Multisite*
555 *Phosphorylation and Function.* Current Biology, 2003. **13**(10): p. 797-806.
556 20. Holz, K.M., et al., *mTOR and S6K1 Mediate Assembly of the Translation Preinitiation*
557 *Complex through Dynamic Protein Interchange and Ordered Phosphorylation Events.*
558 Cell, 2005. **123**(4): p. 569-580.
559 21. Liu, G.Y. and D.M. Sabatini, *mTOR at the nexus of nutrition, growth, ageing and disease.*
560 Nat Rev Mol Cell Biol, 2020. **21**(4): p. 183-203.
561 22. Palmieri, M., et al., *Characterization of the CLEAR network reveals an integrated control*
562 *of cellular clearance pathways.* Hum Mol Genet, 2011. **20**(19): p. 3852-66.

563 23. Calcagnì, A., et al., *Modelling TFE renal cell carcinoma in mice reveals a critical role of*
564 *WNT signaling.* eLife, 2016. **5**.
565 24. Alesi, N., et al., *TFEB drives mTORC1 hyperactivation and kidney disease in Tuberous*
566 *Sclerosis Complex.* Nat Commun, 2024. **15**(1): p. 406.
567 25. Malta, D.C., et al., *<scp>TFEB</scp> and <scp>TFE3</scp> drive kidney cystogenesis*
568 *and tumorigenesis.* EMBO Molecular Medicine, 2023. **15**(5).
569 26. Grahammer, F., et al., *mTORC1 maintains renal tubular homeostasis and is essential in*
570 *response to ischemic stress.* Proceedings of the National Academy of Sciences, 2014.
571 **111**(27): p. E2817-E2826.
572 27. Woo, Y.M., et al., *Profiling of miRNAs and target genes related to cystogenesis in*
573 *ADPKD mouse models.* Sci Rep, 2017. **7**(1): p. 14151.
574 28. Fragiadaki, M., F.M. Macleod, and A.C.M. Ong, *The Controversial Role of Fibrosis in*
575 *Autosomal Dominant Polycystic Kidney Disease.* Int J Mol Sci, 2020. **21**(23).
576 29. Smith, A.O., et al., *The Tumor-Associated Calcium Signal Transducer 2 (TACSTD2)*
577 *oncogene is upregulated in pre-cystic epithelial cells revealing a new target for polycystic*
578 *kidney disease.* medRxiv, 2023.
579 30. Shillingford, J.M. and J.A. Shayman, *Functional TFEB activation characterizes multiple*
580 *models of renal cystic disease and loss of polycystin-1.* Am J Physiol Renal Physiol, 2023.
581 **324**(4): p. F404-F422.
582 31. Muto, Y., et al., *Defining cellular complexity in human autosomal dominant polycystic*
583 *kidney disease by multimodal single cell analysis.* Nature Communications, 2022. **13**(1).
584 32. Sieben, J.C. and C.P. Harris, *Experimental Models of Polycystic Kidney Disease:*
585 *Applications and Therapeutic Testing.* Kidney360, 2023. **4**(8): p. 1155-1173.
586 33. Cui, Z., et al., *Structure of the lysosomal mTORC1-TFEB-Rag-Ragulator megacomplex.*
587 Nature, 2023. **614**(7948): p. 572-579.
588 34. Nojima, H., et al., *The mammalian target of rapamycin (mTOR) partner, raptor, binds the*
589 *mTOR substrates p70 S6 kinase and 4E-BP1 through their TOR signaling (TOS) motif.* J
590 Biol Chem, 2003. **278**(18): p. 15461-4.
591 35. Alesi, N., et al., *TFEB drives mTORC1 hyperactivation and kidney disease in Tuberous*
592 *Sclerosis Complex.* Nature Communications, 2024. **15**(1).
593 36. Woo, M.Y., et al., *Profiling of miRNAs and target genes related to cystogenesis in*
594 *ADPKD mouse models.* Scientific Reports, 2017. **7**(1).
595 37. Kim, K., et al., *Uncoupling protein 1-driven Cre (Ucp1-Cre) is expressed in the epithelial*
596 *cells of mammary glands and various non-adipose tissues.* Mol Metab, 2024. **84**: p.
597 101948.
598 38. Sousa-Filho, B.P.C. and N. Petrovic, *No UCP1 in the kidney.* Molecular Metabolism,
599 2025. **95**: p. 102127.
600 39. Jia, P., et al., *Uncoupling protein 1 inhibits mitochondrial reactive oxygen species*
601 *generation and alleviates acute kidney injury.* EBioMedicine, 2019. **49**: p. 331-340.
602 40. Pravednikova, A.E., et al., *Association of uncoupling protein (Ucp) gene polymorphisms*
603 *with cardiometabolic diseases.* Molecular Medicine 2020 26:1, 2020-05-25. **26**(1).
604 41. Nagai, N., et al., *Uncoupling protein 1 gene −3826 A/G polymorphism is associated with*
605 *weight loss on a short-term, controlled-energy diet in young women.* Nutrition Research,
606 2011. **31**(4): p. 255-261.
607 42. Li, L., et al., *Regulation of mTORC1 by the Rab and Arf GTPases.* Journal of Biological
608 Chemistry, 2010. **285**(26): p. 19705-19709.
609 43. Kim, C.Y., et al., *Rag GTPases are cardioprotective by regulating lysosomal function.*
610 Nature Communications, 2014. **5**(1).
611 44. Efeyan, A., et al., *RagA, but Not RagB, Is Essential for Embryonic Development and Adult*
612 *Mice.* Developmental Cell, 2014. **29**(3): p. 321-329.

613 45. Pearring, N.J., et al., *Loss of Arf4 causes severe degeneration of the exocrine pancreas but*
614 *not cystic kidney disease or retinal degeneration.* PLOS Genetics, 2017. **13**(4): p.
615 e1006740

Acknowledgments

We acknowledge David M. Sabatini and Alejo Efeyan for providing the *RagA/B* mice strain, Kansas PKD Research and Translational Core (U54DK126126), and the Polycystic Kidney Disease Research Resource Consortium (PKD RRC).

Funding

This work was funded by DK094004 and DK127175 (DAG), and TSC Alliance - Grant #1331264 (FFS).

Author contributions

Conceptualization: FFS, ARB, GJP, DAG
Methodology: FFS, ARB, AS, DBA, PT, GJP, DAG
Investigation: FFS, ARB, HL, QC, MG, EK, MSI, AS, DBA, PT.
Data Analysis: FFS, ARB
Supervision: GJP, DAG
Writing—original draft: FFS, AB, GJP, DAG
Writing—review & editing: FFS, ARB, HL, QC, MG, EK, MSI, AS, KS, DBA, PT, GJP, DAG.

Competing interests

The authors declare that they have no competing interests.

Data and materials availability

All data needed to evaluate the conclusions in the paper are present in the paper and/or the Supplementary Materials.

Figures and Tables

Figure Legends

Figure 1. *RagA/B* deletion in kidney tubular epithelial cells promotes a striking polycystic phenotype. (A) Representative image from *RagA/B* floxed control and *Ksp*-Cre;*RagA/B* male mice kidney morphology and **(B)** Whole kidney H&E sections from 4 to 12 weeks of age. Scale bars = 500 µm. **(C)** Kidneys/body weight ratio from 2 to 12 weeks of age. **(D)** H&E sections showing cyst's location within the kidney cortex and medulla. Scale bars = 50 µm. **(E)** Low (top) and high (bottom) magnification of Mason's Trichrome stained kidneys showing collagen accumulation (blue) in *Ksp*-Cre;*RagA/B* at 8 weeks of age. Scale bars = 50 µm (top) and 20 µm (bottom). **(F)** Inflammation markers gene expression at 8 weeks of age. **(G)** Blood urea nitrogen (BUN) serum levels from 2 to 12 weeks of age. **(H)** Kaplan-Meier curve showing survival of *Ksp*-Cre;*RagA/B* (n = 8) relative to the floxed controls (n=8). White bars = *RagA/B* floxed control, n = 7-10; green bars = *Ksp*-Cre;*RagA/B*, n = 3-10. In **C**, **F**, and **G,** data are presented as mean ± SEM. *p<0.05, **p<0.01, and ****p<0.0001 versus the respective timepoint floxed control (unpaired Student t-test); ns = p>0.05.

Figure 2. Cystogenesis is not dependent on mTORC1 activation. (A) *RagA* and *RagB* gene expression in kidneys of *RagA/B* floxed control and *Ksp*-Cre;*RagA/B* male mice at 6 weeks of age. **(B)** Western blotting confirmed reduced RagA and RagB protein content and mTORC1 downstream proteins. **(C)** p-S6 is low or not expressed in cyst lining cells. IHC sections of *RagA/B* floxed control and *Ksp*-Cre;*RagA/B* male mice at 2, 4, and 8 weeks of age. Scale bars = 20 µm. White bars = *RagA/B* floxed control, n = 6; green bars = *Ksp*-Cre;*RagA/B* , n = 5. In **A,** the data are presented as mean ± SEM. ***p<0.001 versus the respective timepoint floxed control (unpaired Student *t*-test).

Figure 3. TFEB is the driver of kidney cystogenesis. (A) TFEB localization throughout cyst progression at 2, 4, and 8 weeks of age. **(B)** Heatmaps portraying TFEB CLEAR target gene set expression differences (Log2FoldChange) between *RagA/B* floxed controls and *Ksp*-Cre;*RagA/B* male mice at 6 weeks of age. **(C)** WNT signaling gene set expression differences (Log2FoldChange) between *RagA/B* floxed controls and *Ksp*-Cre;*RagA/B* male mice at 6 weeks of age. **(D)** Whole kidney lysate western blotting for β-catenin at 4 and 8 weeks of age. **(E)** β-catenin IHC sections of *RagA/B* floxed control and *Ksp*-Cre;*RagA/B* male mice at 8 weeks of age. Scale bars = 20 µm.

Figure 4. Reduced efficacy of rapamycin in *Ksp*-Cre;*RagA/B* mice compared to *Ksp*-Cre;*Tsc2* mice. (A) GSEA comparison of molecular hallmarks from whole kidney bulk-RNAseq of *Ksp*-Cre;*RagA/B* and *Ksp*-Cre;*Tsc2* kidneys (only includes hallmarks with FDR q-val </= 0.05 in the *Ksp*-Cre;*RagA/B* dataset). **(B)** Kidneys/body weight ratio at P50 (floxed control + vehicle, n = 10; *Ksp-Cre;RagA/B* + vehicle , n = 3; floxed control + rapamycin, n = 10; *Ksp*-Cre;*RagA/B* + vehicle , n = 7). **(C)** Representative whole kidney sections from *RagA/B* floxed control and *Ksp*-Cre;*RagA/B* treated with vehicle or rapamycin 1.0 mg/Kg at P50. Scale bars = 500 µm. **(D)** p-S6 and TFEB IHC kidney sections from *RagA/B* floxed control and *Ksp*-Cre;*RagA/B* male mice treated with vehicle or Rapamycin 1.0 mg/kg. Scale bars = 20 µm. White bars = *RagA/B* floxed control; green bars = *Ksp*-Cre;*RagA/B*. In **B,** data are presented as mean ± SEM. ****p<0.0001 versus the respective treated floxed control–genotype effect (Two-Way ANOVA).

Figure 5. *Tfeb* is required for cyst formation downstream of *RagA/B* loss. (A) Representative image from *RagA/B;Tfeb* floxed control and *Ksp*-Cre;*RagA/B;Tfeb* male mice kidney morphology at 6 weeks of age. **(B)** Kidneys/body weight ratio (*RagA/B;Tfeb* floxed control, n = 8; *Ksp*-Cre*;RagA/B;Tfeb*, n = 9). **(C)** Kidney H&E sections showing absence of cysts. Scale bars = 500 µm (whole kidney), 50 µm (cortex and medulla sections). **(D)** Blood urea nitrogen (BUN) serum from *RagA/B;Tfe*b floxed control and *Ksp*-Cre;*RagA/B;Tfeb* levels at 6 weeks of age. **(E)** TFEB IHC sections of *RagA/B;Tfeb* floxed control and *Ksp*-Cre;*RagA/B;Tfeb* male mice at 6 weeks of age. Scale bars = 20 µm. **(F)** Expression of TFEB target genes *Atg9b* and *Ctsd* (*RagA/B* floxed control, n = 6; *Ksp*-Cre;*RagA/B* n = 5; *RagA/B;Tfeb* floxed control, n = 5; *Ksp*-Cre;*RagA/B;Tfeb*, n = 4; *Raptor* floxed control, n = 5; *Ksp*-Cre;*Raptor*, n = 4). **(G)** Whole kidney lysate western blotting for mTORC1 downstream proteins. **(H) p**-S6 IHC sections of *RagA/B;Tfeb* floxed control and *Ksp*-Cre;*RagA/B;Tfeb* male mice at 6 weeks of age. Scale bars = 20 µm. **(I) p**-AKT IHC sections of *RagA/B;Tfeb* floxed control and *Ksp*-Cre;*RagA/B;Tfeb* male mice at 6 weeks of age. Scale bars = 20 µm. White bars = *RagA/B, RagA/B;Tfeb* or *Raptor* floxed controls; green bars = *Ksp*-Cre;*RagA/B*; blue bars = *Ksp*-Cre;*RagA/B;Tfeb*; pink bars = *Ksp*-Cre;*Raptor*. In **B**, **D**, and **F,** data are presented as mean ± SEM. p values versus the respective floxed control (unpaired Student *t*-test).

Figure 6. Rag GTPase, not mTORC1, is the main TFEB suppressor *in vivo.* (A) Representative image from *Raptor* floxed control and *Ksp*-Cre;*Raptor* male mice kidney morphology at 6 weeks of age. **(B)** Kidneys/body weight ratio and **(C)** H&E sections showing absence of cysts. Scale bars = 500 µm (whole kidney), 50 µm (cortex and medulla sections). **(D)** Blood urea nitrogen (BUN) serum from *Raptor* floxed control and *Ksp*-Cre;*Raptor* levels at 6 weeks of age. **(E)** p-S6 IHC, **(F)** p-AKT, and **(G)** TFEB IHC sections of *Raptor* floxed control and *Ksp*-Cre;*Raptor* male mice at 6 weeks of age. Scale bars = 20 µm. **(H)** Whole kidney lysate western blotting for mTORC1 downstream proteins. White bars = *Raptor* floxed control, n = 4; pink bars = *Ksp*-Cre;*Raptor,* n = 5. In **B** and **D,** data are presented as mean ± SEM. p values versus the floxed control (unpaired Student *t*-test).

Figure 7. RagA/B deletion overlaps with ADPKD models, with TFEB activation as a consistent biomarker. (A) GSEA comparison of molecular hallmarks from whole kidney bulk-RNAseq of *Ksp*-Cre;*RagA/B* and *HoxB7-Cre;Pkd1* (left) or *HoxB7*-Cre;*Pkd2* (right) kidneys (only includes hallmarks with FDR q-val </= 0.05 in the *Ksp-Cre;RagA/B* dataset). **(B)** Heatmaps portraying PKD-associated genes expression differences (Log2FoldChange) between *RagA/B* floxed controls and *Ksp*-Cre;*RagA/B* male mice at 6 weeks of age. **(C)** Representative TFEB and p-S6 IHC from *Pkd1*$^{fl/fl}$ and *Pax8-rTTA;Tet-O-7*-Cre;*Pkd1*$^{fl/fl}$ male mice and **(D)** kidney sections from ADPKD patients. Scale bars = 20 µm.

Figures

Figure 1.

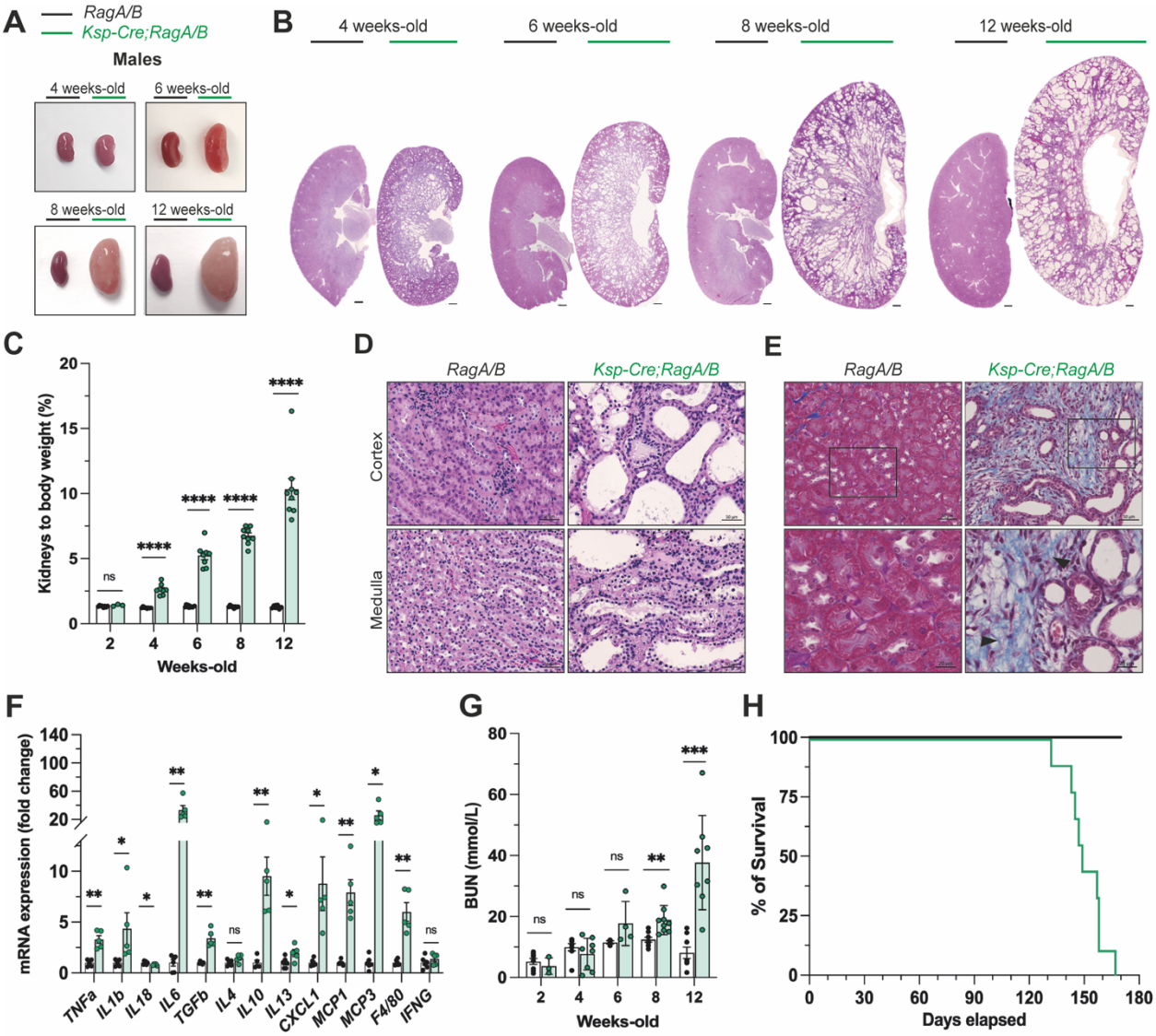

Figure 2.

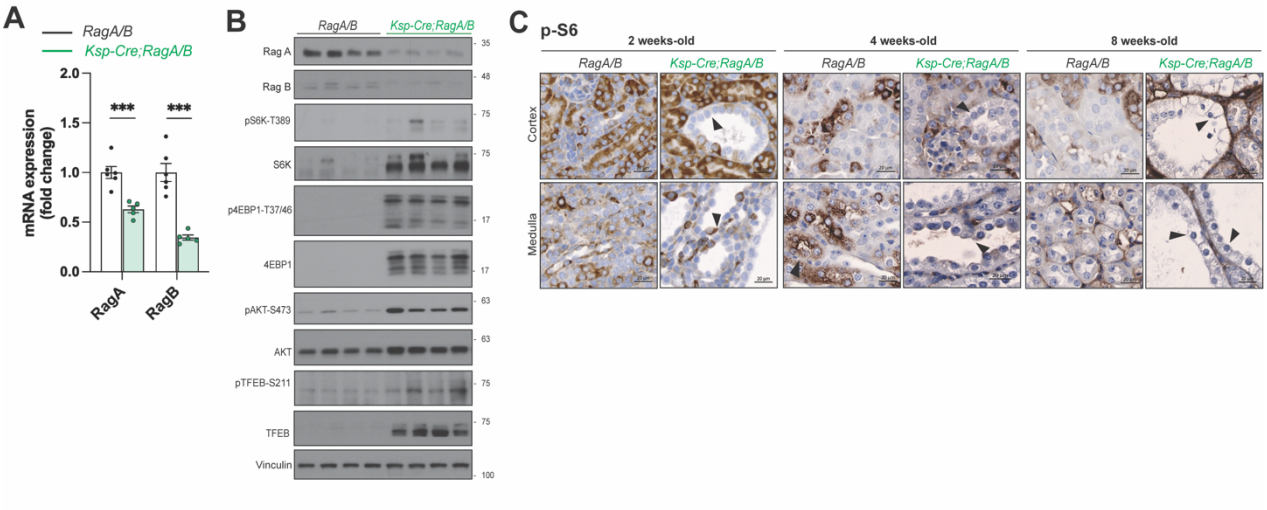
A
RagA/B
Ksp-Cre;RagA/B
mRNA expression (fold change)
2.0
1.5
1.0
0.5
0.0
***
***
RagA
RagB
B
RagA/B
Ksp-Cre;RagA/B
Rag A
Rag B
pS6K-T389
S6K
p4EBP1-T37/46
4EBP1
pAKT-S473
AKT
pTFEB-S211
TFEB
Vinculin
35
48
75
75
17
17
63
63
75
75
100
C
p-S6
2 weeks-old
4 weeks-old
8 weeks-old
RagA/B
Ksp-Cre;RagA/B
RagA/B
Ksp-Cre;RagA/B
RagA/B
Ksp-Cre;RagA/B
Cortex
Medulla

Figure 3.

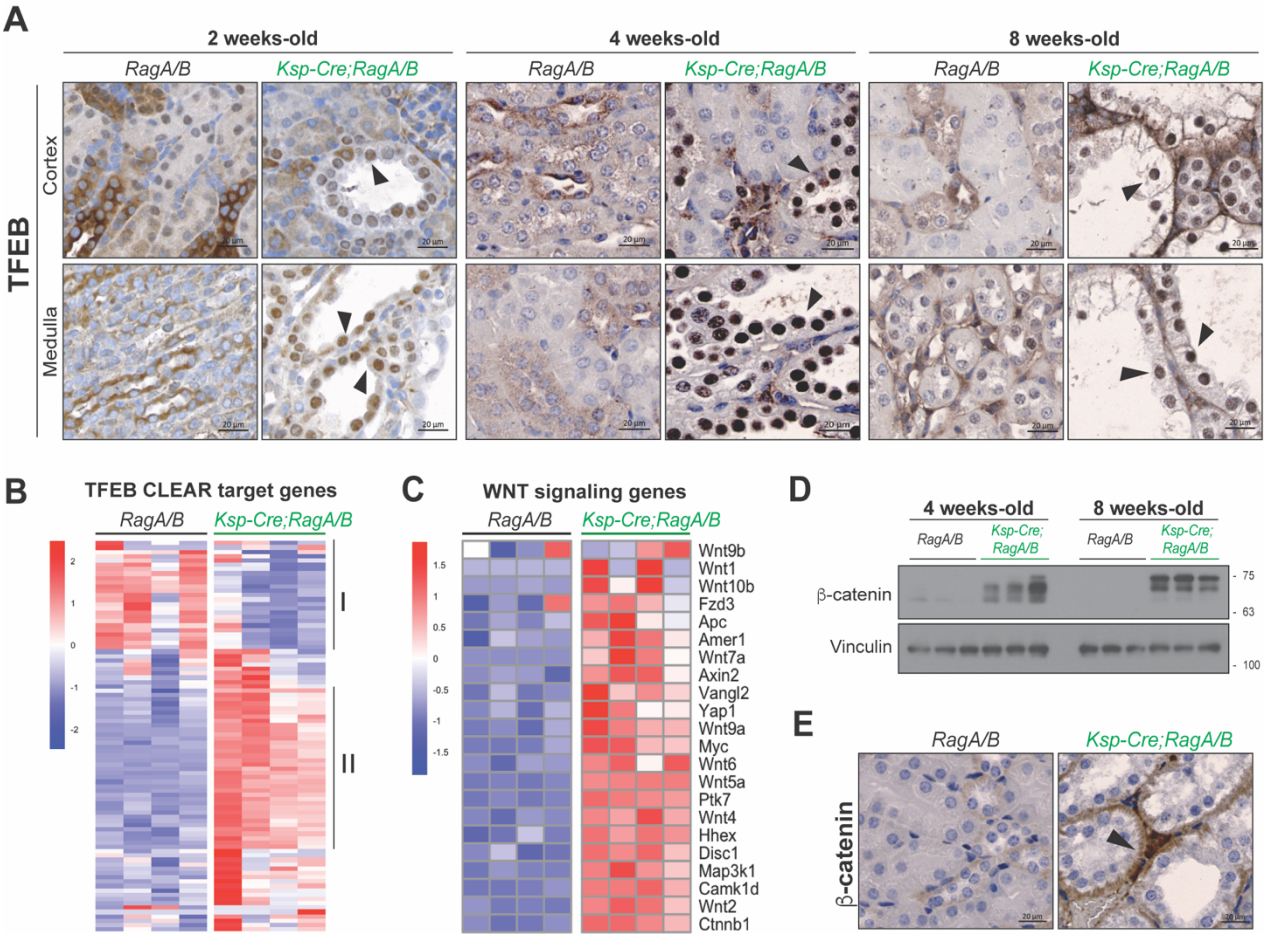
A
2 weeks-old
4 weeks-old
8 weeks-old
RagA/B
Ksp-Cre;RagA/B
TFEB
Cortex
Medulla
B
TFEB CLEAR target genes
I
II
C
WNT signaling genes
Wnt9b
Wnt1
Wnt10b
Fzd3
Apc
Amer1
Wnt7a
Axin2
Vangl2
Yap1
Wnt9a
Myc
Wnt6
Wnt5a
Ptk7
Wnt4
Hhex
Disc1
Map3k1
Camk1d
Wnt2
Ctnnb1
D
β-catenin
Vinculin
75
63
100
E
β-catenin

Figure 4.

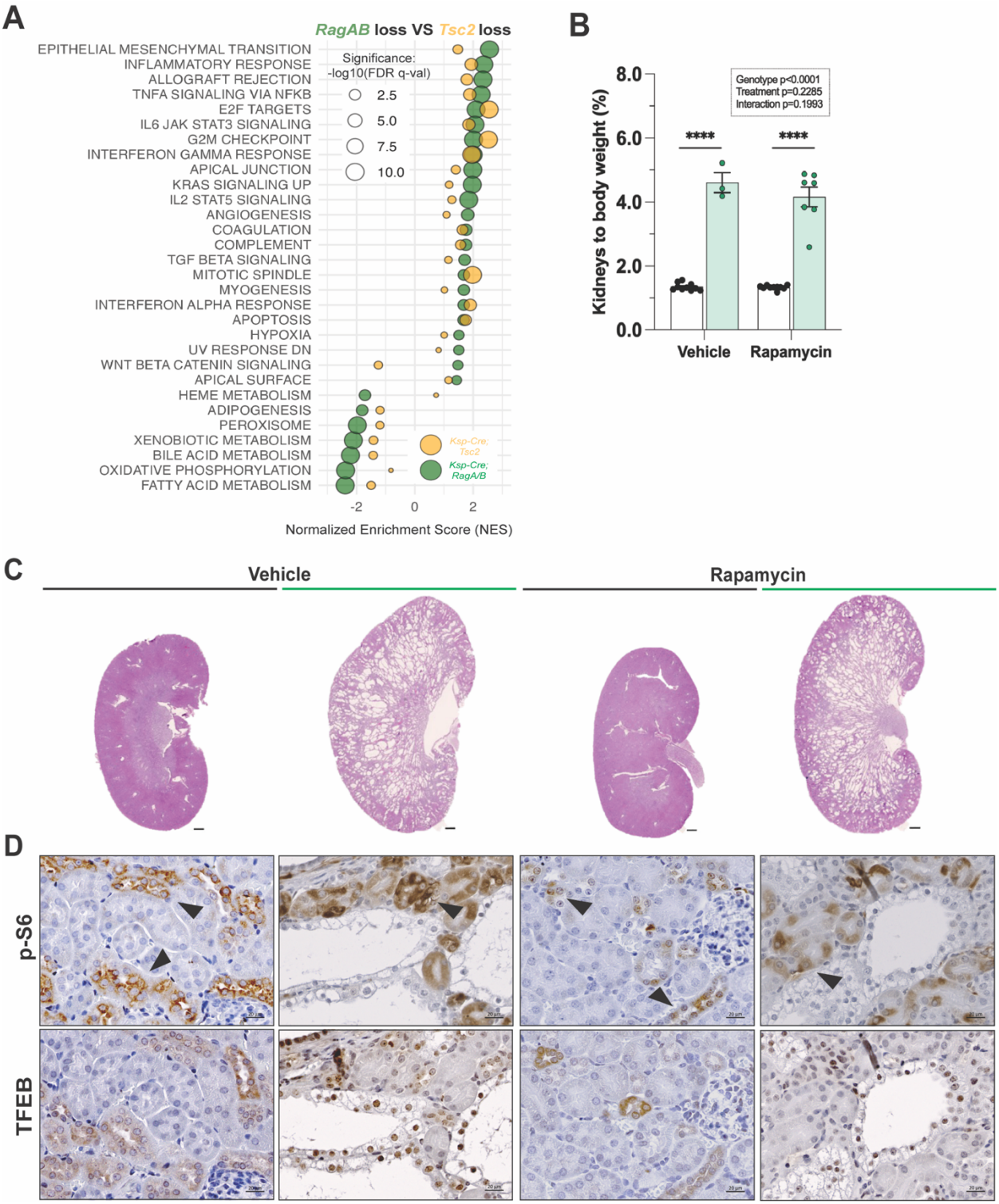
A
RagAB loss VS Tsc2 loss
EPITHELIAL MESENCHYMAL TRANSITION
INFLAMMATORY RESPONSE
ALLOGRAFT REJECTION
TNFA SIGNALING VIA NFKB
E2F TARGETS
IL6 JAK STAT3 SIGNALING
G2M CHECKPOINT
INTERFERON GAMMA RESPONSE
APICAL JUNCTION
KRAS SIGNALING UP
IL2 STAT5 SIGNALING
ANGIOGENESIS
COAGULATION
COMPLEMENT
TGF BETA SIGNALING
MITOTIC SPINDLE
MYOGENESIS
INTERFERON ALPHA RESPONSE
APOPTOSIS
HYPOXIA
UV RESPONSE DN
WNT BETA CATENIN SIGNALING
APICAL SURFACE
HEME METABOLISM
ADIPOGENESIS
PEROXISOME
XENOBIOTIC METABOLISM
BILE ACID METABOLISM
OXIDATIVE PHOSPHORYLATION
FATTY ACID METABOLISM
Significance:
-log10(FDR q-val)
2.5
5.0
7.5
10.0
Ksp-Cre; Tsc2
Ksp-Cre; RagA/B
-2
0
2
Normalized Enrichment Score (NES)
B
Kidneys to body weight (%)
8.0
6.0
4.0
2.0
0.0
Genotype p<0.0001
Treatment p=0.2285
Interaction p=0.1993
****
****
Vehicle
Rapamycin
C
Vehicle
Rapamycin
D
p-S6
TFEB

Figure 5.

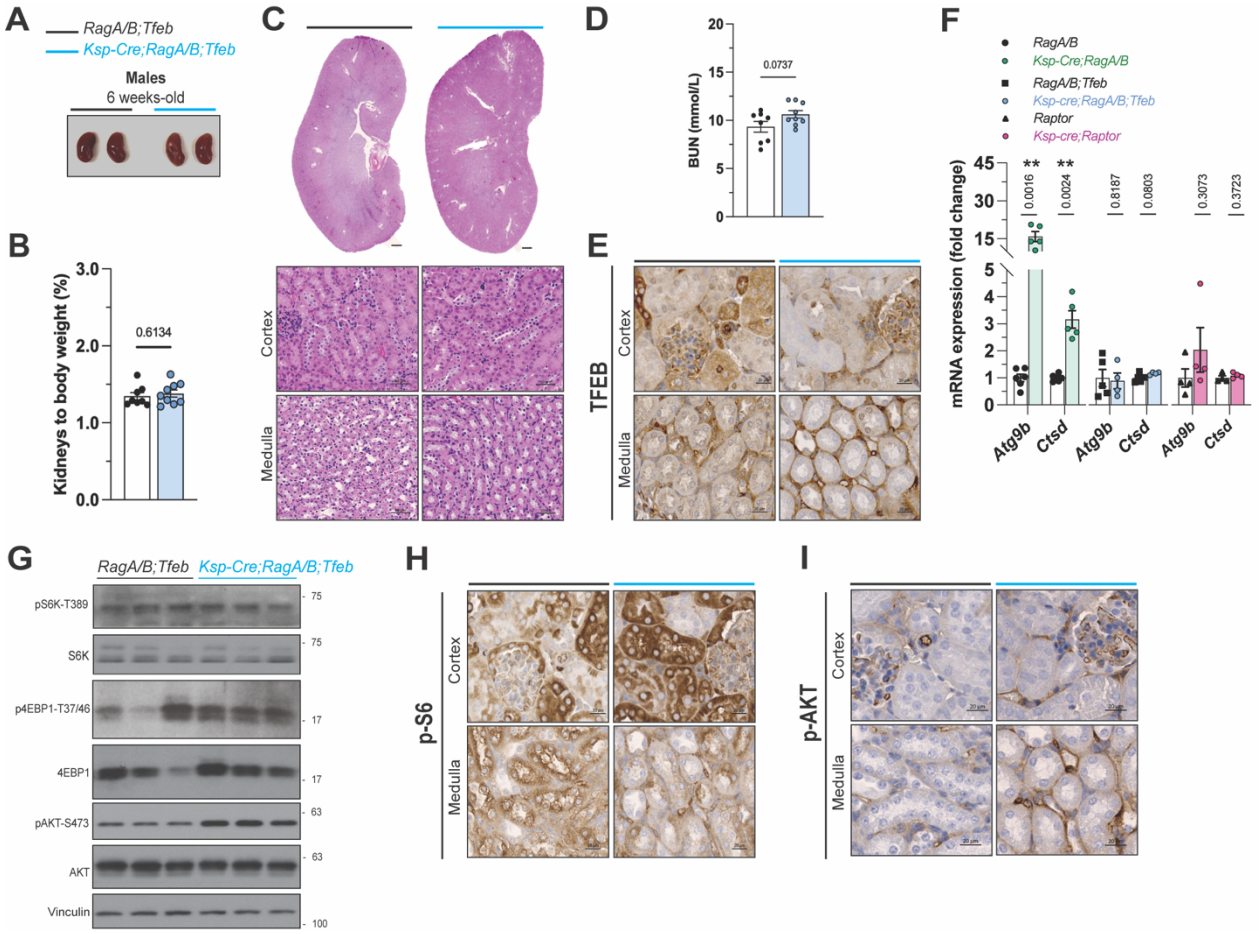
A
RagA/B;Tfeb
Ksp-Cre;RagA/B;Tfeb
Males
6 weeks-old
B
Kidneys to body weight (%)
0.6134
C
Cortex
Medulla
D
BUN (mmol/L)
0.0737
E
TFEB
Cortex
Medulla
F
RagA/B
Ksp-Cre;RagA/B
RagA/B;Tfeb
Ksp-cre;RagA/B;Tfeb
Raptor
Ksp-cre;Raptor
mRNA expression (fold change)
0.0016
0.0024
0.8187
0.0803
0.3073
0.3723
Atg9b
Ctsd
G
RagA/B;Tfeb
Ksp-Cre;RagA/B;Tfeb
pS6K-T389
S6K
p4EBP1-T37/46
4EBP1
pAKT-S473
AKT
Vinculin
H
p-S6
Cortex
Medulla
I
p-AKT
Cortex
Medulla

Figure 6.

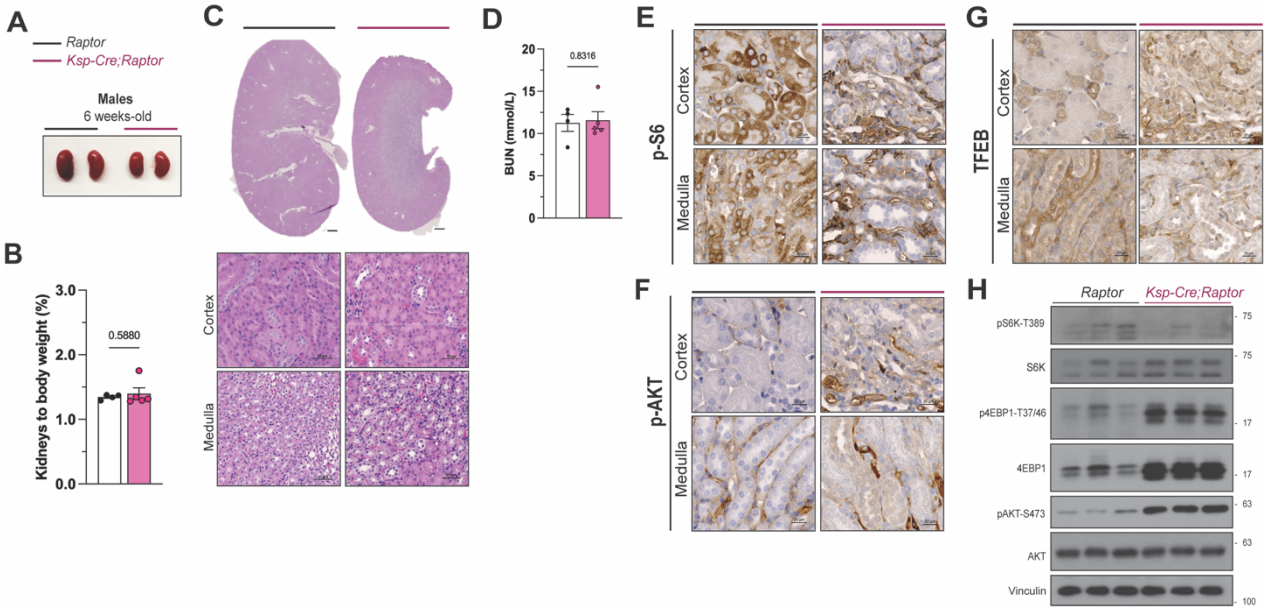
A
Raptor
Ksp-Cre;Raptor
Males
6 weeks-old
B
Kidneys to body weight (%)
3.0
2.0
1.0
0.0
0.5880
C
Cortex
Medulla
D
BUN (mmol/L)
20
15
10
5
0
0.8316
E
p-S6
Cortex
Medulla
F
p-AKT
Cortex
Medulla
G
TFEB
Cortex
Medulla
H
Raptor
Ksp-Cre;Raptor
pS6K-T389
S6K
p4EBP1-T37/46
4EBP1
pAKT-S473
AKT
Vinculin
75
75
17
17
63
63
100

Figure 7.

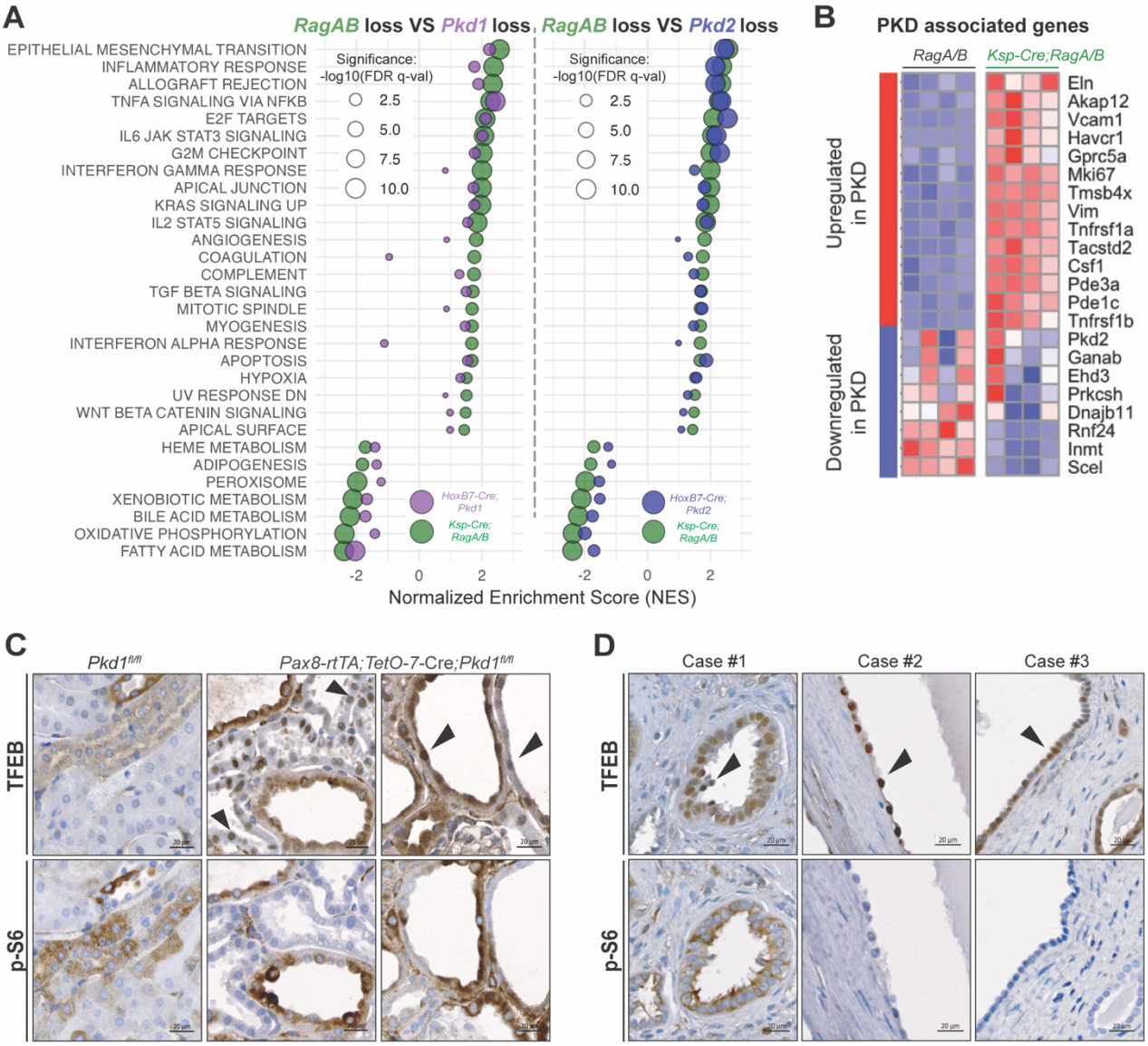
A
RagAB loss VS Pkd1 loss
RagAB loss VS Pkd2 loss
EPITHELIAL MESENCHYMAL TRANSITION
INFLAMMATORY RESPONSE
ALLOGRAFT REJECTION
TNFA SIGNALING VIA NFKB
E2F TARGETS
IL6 JAK STAT3 SIGNALING
G2M CHECKPOINT
INTERFERON GAMMA RESPONSE
APICAL JUNCTION
KRAS SIGNALING UP
IL2 STAT5 SIGNALING
ANGIOGENESIS
COAGULATION
COMPLEMENT
TGF BETA SIGNALING
MITOTIC SPINDLE
MYOGENESIS
INTERFERON ALPHA RESPONSE
APOPTOSIS
HYPOXIA
UV RESPONSE DN
WNT BETA CATENIN SIGNALING
APICAL SURFACE
HEME METABOLISM
ADIPOGENESIS
PEROXISOME
XENOBIOTIC METABOLISM
BILE ACID METABOLISM
OXIDATIVE PHOSPHORYLATION
FATTY ACID METABOLISM
Significance:
-log10(FDR q-val)
2.5
5.0
7.5
10.0
HoxB7-Cre; Pkd1
Ksp-Cre; RagA/B
HoxB7-Cre; Pkd2
Ksp-Cre; RagA/B
-2
0
2
Normalized Enrichment Score (NES)
B
PKD associated genes
RagA/B
Ksp-Cre;RagA/B
Upregulated in PKD
Downregulated in PKD
Eln
Akap12
Vcam1
Havcr1
Gprc5a
Mki67
Tmsb4x
Vim
Tnfrsf1a
Tacstd2
Csf1
Pde3a
Pde1c
Tnfrsf1b
Pkd2
Ganab
Ehd3
Prkcsh
Dnajb11
Rnf24
Inmt
Scel
C
Pkd1fl/fl
Pax8-rtTA;TetO-7-Cre;Pkd1fl/fl
TFEB
p-S6
D
Case #1
Case #2
Case #3
TFEB
p-S6